



# Effects of Different Fast Periodic Excitations on the Pitchfork Bifurcation and Vibrational Resonance

Jiaqi Zhang, Jianhua Yang<sup>\*,†</sup>, Zhencai Zhu and Gang Shen  
*School of Mechatronic Engineering,  
China University of Mining and Technology,  
Xuzhou, Jiangsu 221116, P. R. China*

*\*Jiangsu Key Laboratory of Mine Mechanical and Electrical Equipment,  
China University of Mining and Technology,  
Xuzhou 221116, P. R. China  
†jianhuayang@cumt.edu.cn*

Miguel A. F. Sanjuán  
*Departamento de Física, Universidad Rey Juan Carlos,  
Tulipán s/n, 28933 Móstoles, Madrid, Spain  
Department of Applied Informatics, Kaunas University of Technology,  
Studentu 50-415, Kaunas LT-51368, Lithuania*

Received September 1, 2019

We investigate the effects on the pitchfork bifurcation and the vibrational resonance of an overdamped bistable system subjected to both a slow harmonic excitation and a fast periodic excitation with different waveforms. We use numerical simulations along with theoretical explanations to analyze some interesting phenomena. The bifurcation configuration depends closely on the form of the fast excitation. As a result, we have found that the key factor to influence the bifurcation configuration is the symmetry property of the fast excitation. Further, due to the relationship of the vibrational resonance with the pitchfork bifurcation, the vibrational resonance also depends closely on the form of the fast periodic excitation. Moreover, for anharmonic fast excitations, if it is asymmetric, the vibrational resonance usually depends closely on the initial conditions.

*Keywords:* Pitchfork bifurcation; vibrational resonance; overdamped bistable system; fast periodic excitation.

## 1. Introduction

Bifurcations refer to a change of the equilibria of a system, and when they occur, the behavior of a system may change suddenly with unpredictable consequences. One of the bifurcations that typically occur in dynamical systems is the pitchfork bifurcation (PB), which furthermore is related to the well-known phenomenon of vibrational resonance (VR)

[Landa & McClintock, 2000; Ji & Leung, 2002; Popov, 2003; Rajasekar & Sanjuán, 2016]. By using numerical simulations, Landa and McClintock found that there was a nonlinear relationship between the response amplitude of the system at the low-frequency (slow) excitation and the amplitude of the high-frequency (fast) excitation. By adjusting the fast excitation, the weak slow excitation

---

<sup>†</sup>Author for correspondence

is enhanced to a great extent [Ullner et al., 2003; Chizhevsky & Giacomelli, 2008; Rajasekar et al., 2012; Wang et al., 2014]. They coined this phenomenon as Vibrational Resonance (VR). Both the PB and VR are important topics in nonlinear dynamics.

A bistable system is typically used to investigate the PB and VR [Blekhman & Landa, 2004; Thomsen, 2008; Rajasekar et al., 2010; Yao & Zhan, 2010; Yang et al., 2015; Yang et al., 2018]. To our knowledge, there is very little work on how the waveform of the fast excitation can influence the PB configuration and VR. However, in the practice of engineering, fast excitations appear usually in different waveforms [Grassie et al., 1982; Yabuno et al., 2004; Yabuno & Tsumoto, 2007; Mares et al., 2013]. As a result, it would be necessary to study the effect of the waveform of the fast excitation on PB and VR. Due to the difficulty in solving analytically the nonlinear response under complicated excitations, we study PB and VR mainly by numerical simulations. Some analytical results in former works [Blekhman, 2000; Blekhman & Landa, 2004; Yang & Zhu, 2012] will be given as auxiliary explanations.

The paper is organized as follows. In Sec. 2, we will study the PB configuration induced by different periodic fast excitations. In Sec. 3, we will study the VR influenced by the waveform of the fast excitation. In the last section, the main conclusions of the paper are summarized.

## 2. Fast Excitation Forms on PB

We study the typical overdamped bistable system

$$\frac{dx}{dt} = ax - bx^3 + f \cos \omega t + Fu(t). \quad (1)$$

Both  $a$  and  $b$  are system parameters. To make the problem simpler, we fix  $a = 1$  and  $b = 1$ . The term  $f \cos \omega t$  corresponds to a slow excitation with frequency  $\omega$  and amplitude  $f$ .  $Fu(t)$  represents an auxiliary fast periodic excitation with amplitude  $F$ . We consider the periodic function  $u(t)$  having either a harmonic or an anharmonic waveform. If the period of  $u(t)$  is  $\frac{2\pi}{\Omega}$ , we define  $\omega \ll \Omega$ . In addition, we assume  $f \ll 1$ . In the following analysis, we fix  $\omega = 0.1$ ,  $\Omega = 10$ ,  $f = 0.01$ .

For the function  $u(t)$ , we will use six typical periodic waveforms and their expressions as follows [Gandhimathi et al., 2006].

### Cosine waveform

$$u(t) = \cos \Omega t. \quad (2)$$

### Square waveform

$$u(t) = \begin{cases} 1, & 0 \leq t < \frac{\pi}{\Omega}, \\ -1, & \frac{\pi}{\Omega} \leq t < \frac{2\pi}{\Omega}. \end{cases} \quad (3)$$

### Asymmetric sawtooth waveform

$$u(t) = \frac{\Omega t}{\pi} - 1, \quad 0 \leq t < \frac{2\pi}{\Omega}. \quad (4)$$

### Symmetric sawtooth waveform

$$u(t) = \begin{cases} \frac{2\Omega t}{\pi} - 1, & 0 \leq t < \frac{\pi}{\Omega}, \\ -\frac{2\Omega t}{\pi} + 3, & \frac{\pi}{\Omega} \leq t < \frac{2\pi}{\Omega}. \end{cases} \quad (5)$$

### Modulus of sine waveform

$$u(t) = \left| \sin \frac{\Omega t}{2} \right|. \quad (6)$$

### Rectified cosine waveform

$$u(t) = \begin{cases} \cos \Omega t, & 0 \leq t < \frac{\pi}{2\Omega} \quad \text{or} \quad \frac{3\pi}{2\Omega} \leq t < \frac{2\pi}{\Omega} \\ 0, & \frac{\pi}{2\Omega} \leq t < \frac{3\pi}{2\Omega}. \end{cases} \quad (7)$$

Graphical representations of the above six waveforms are shown in Fig. 1.

We will show the PB diagram by using numerical simulations for the six periodic waveforms  $u(t)$ . The numerical method for calculating the stable equilibrium point is given in our previous work [Yang et al., 2015, Eqs. (14)–(18)]. Nevertheless, we will mention it briefly here. For a function  $f(x)$ , the Fourier series expanded in  $[0, 2\pi]$  is as follows

$$f(x) = \frac{a_0}{2} + \sum_{n=1}^{\infty} (a_n \cos nx + b_n \sin nx). \quad (8)$$

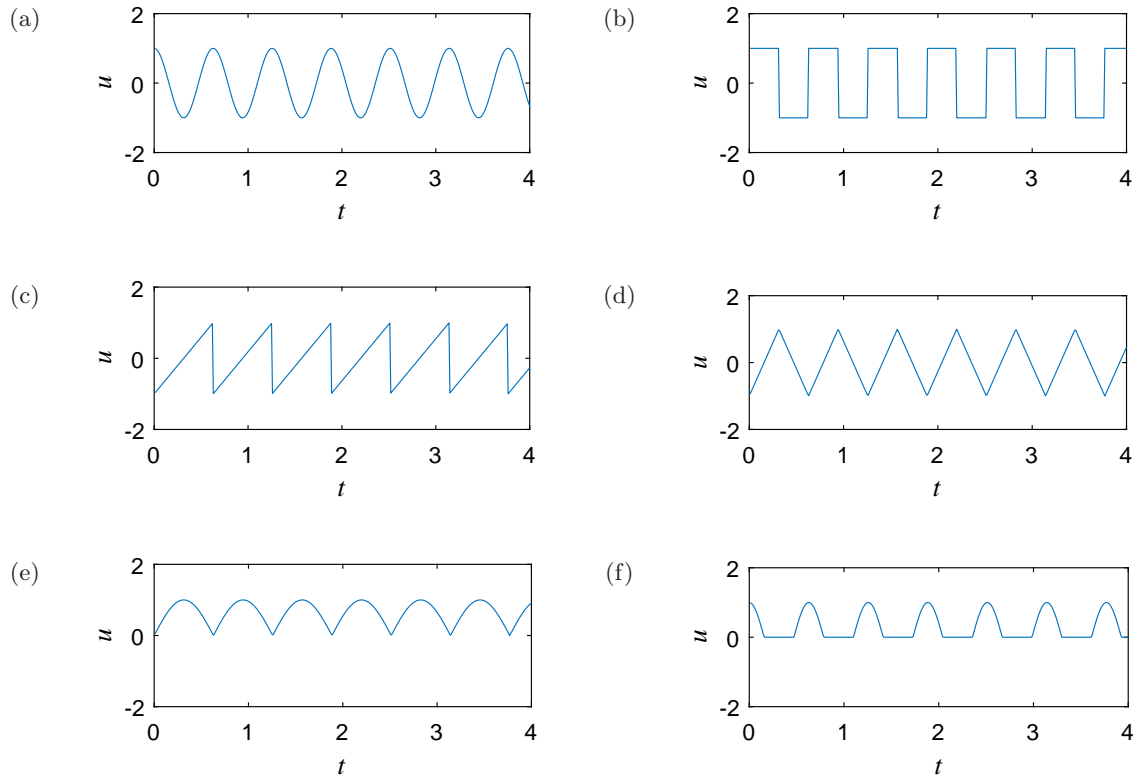


Fig. 1. Curves of six different periodic waveforms. (a) Cosine waveform, (b) square waveform, (c) asymmetric sawtooth waveform, (d) symmetric sawtooth waveform, (e) modulus of sine waveform and (f) rectified cosine waveform.

In Eq. (8), the coefficients of the Fourier components are

$$\begin{cases} a_n = \frac{1}{\pi} \int_0^{2\pi} f(x) \cos(nx) dx & (n = 0, 1, 2, \dots), \\ b_n = \frac{1}{\pi} \int_0^{2\pi} f(x) \sin(nx) dx & (n = 0, 1, 2, \dots). \end{cases} \quad (9)$$

In Eq. (9), the constant component is

$$\frac{a_0}{2} = \frac{1}{2\pi} \int_0^{2\pi} f(x) dx. \quad (10)$$

Since the time series  $x(t)$  cannot be described by a specific function, the constant component can be computed numerically,

$$X^* = \frac{a_0}{2} = \frac{1}{rT} \int_0^{rT} x(t) dt. \quad (11)$$

In fact, the constant component of the time series is the stable equilibrium of the response, i.e.  $X^*$  in Eq. (11). The discrete form of Eq. (11) is

$$X^* = \frac{1}{rT} \sum_{i=1}^N (x(t_i) \Delta t), \quad N = \frac{rT}{\Delta t}. \quad (12)$$

In Eq. (12),  $x(t)$  represents the time series with total time  $T$  and interval  $\Delta t$ .

The analytical method is based on the method of direct separation of fast and slow motions. In previous work, the analytical method has been validated and its result is shown in Eq. (13). Considering that the derivation of the analytical method is rather complicated and it is not the objective of this paper, we will show the bifurcation curve by analytical results only for  $u(t)$  in the cosine waveform. The analytical result is as follows [Yang & Zhu, 2012, Eqs. (7)–(13)]

$$X^* = 0, \quad X_{\pm}^* = \pm \sqrt{\frac{-C_1}{b}}, \quad (13)$$

where

$$\begin{cases} C_1 = -a + \frac{3bF^2}{2\mu^2}, \\ \mu^2 = \left(-a + \Omega \cos \frac{\pi}{2}\right)^2 + \left(\Omega \sin \frac{\pi}{2}\right)^2. \end{cases} \quad (14)$$

In Eq. (13), the former  $X^* = 0$  is the unstable equilibrium of the response, while the latter  $X^*$  is the stable equilibrium of the response.

Based on the above numerical and analytical solutions, Fig. 2 is plotted to illustrate the diagram of the equilibrium points. The black solid line in panel Fig. 2(a) is plotted by using the analytical method, as an example. It can be seen that the theoretical analysis is in good agreement with the numerical simulations, showing the reliability of the method. Additionally, we find that the panels Figs. 2(c), 2(e) and 2(f) have a deformed bifurcation phenomenon. Specifically, for the cosine waveform, square waveform, symmetric sawtooth waveform cases, the PB diagram is symmetric, as shown in Figs. 2(a), 2(b) and 2(d). However, for the asymmetric sawtooth waveform, modulus of sine waveform, rectified waveform cases, the asymmetry of the fast excitations breaks the symmetry of the PB diagram. Moreover, we assume that there is a jump phenomenon, so we enlarge the breaking parts in the panels Figs. 2(c), 2(e) and 2(f) locally as shown in Fig. 3.

As shown in Fig. 3, even if panel Fig. 2(c) is enlarged ten thousand times, it is still difficult to determine the specific position of its accurate bifurcation point, which indicates that the bifurcation diagram corresponding to the excitation in Fig. 1(c) has a jumping process. However, the bifurcation points corresponding to excitations in Figs. 1(e) and 1(f) can be determined with a relative accuracy.

Due to the complexity of the excitations, it will be difficult to determine the position of the equilibrium points by the analytical method. In order to make the results more convincing, we plot the phase diagram to do another verification as shown in Fig. 4. In this figure, each signal corresponds to two panels. One corresponds before the bifurcation and the other one after the bifurcation. It can be seen that each numerically calculated equilibrium point (the small circle) is located at the center of the corresponding phase curve. Hence, the phase diagram verifies the correctness of Fig. 2 again.

Next, we use the cosine waveform to study the bifurcation diagram. Figure 5 shows six cosine waveforms, which are converted slightly from the signal shown in Eq. (4). Here, we define a deviated cosine function

$$u(t) = \cos \Omega t + \delta, \tag{15}$$

where the constant  $\delta$  indicates the deviation. The deviated cosine waveform excitations given in Fig. 5 are used as fast excitations, and the corresponding PB diagrams are shown in Fig. 6.

Apparently, as illustrated in Fig. 6, the deviation  $\delta$  will break the symmetry of the PB configuration. If  $\delta > 0$ , the bifurcation point will move upwards, and the critical value of  $F$  corresponding to the PB point will decrease. Conversely, if  $\delta < 0$ , the bifurcation point will move downwards, and the critical value of  $F$  will also decrease.

For the square waveforms, Fig. 7 shows six kinds of square waveforms with different duty cycle values [Nakamura *et al.*, 2013], whose mathematical expressions are shown in Eq. (16),

$$u(t) = \begin{cases} 1, & 0 \leq t < \frac{2R\pi}{\Omega} \\ -1, & \frac{2R\pi}{\Omega} \leq t < \frac{2\pi}{\Omega}. \end{cases} \tag{16}$$

Here, the duty cycle is defined as the ratio between the pulse duration, or pulse width and the period of a rectangular waveform. We use the symbol  $R$  as the duty cycle. When  $R = 0.5$ , we have the standard square waveform as shown in Fig. 1(b).

The waveforms in Fig. 7 are used as fast excitations and the corresponding PB diagrams are shown in Fig. 8. Further, in Fig. 8, we have similar results to those in Fig. 6. Specifically, the bifurcation point will move upwards when  $R > 0.5$ , and the bifurcation point will move downwards when  $R < 0.5$ . The critical value of  $F$  at the bifurcation point will decrease when  $R \neq 0.5$ . The greater the value of  $R$  from 0.5, the more the difference of the PB configuration diagram from the standard PB bifurcation diagram.

Consider the sawtooth waveforms with different rising edge slopes, denoted by  $k$ , whose mathematical expressions are shown in Eq. (17),

$$u(t) = \begin{cases} kt - 1, & 0 \leq t < \frac{2}{k} \\ \frac{\Omega kt - \Omega - \pi k}{\Omega - \pi k}, & \frac{2}{k} \leq t < \frac{2\pi}{\Omega}. \end{cases} \tag{17}$$

Figure 9 shows six sawtooth waveforms with different values of  $k$ . In Fig. 9(c), the rising edge slope equals the negative value of the slope of descending edge. It is the standard symmetric sawtooth waveform. In other subplots of Fig. 9, the waveform degenerates to the asymmetric sawtooth waveform.

The waveforms given in Fig. 9 are used as fast excitations and the corresponding PB diagrams are shown in Fig. 10. The results in Fig. 10 show that the rising/descending edge slopes influence the

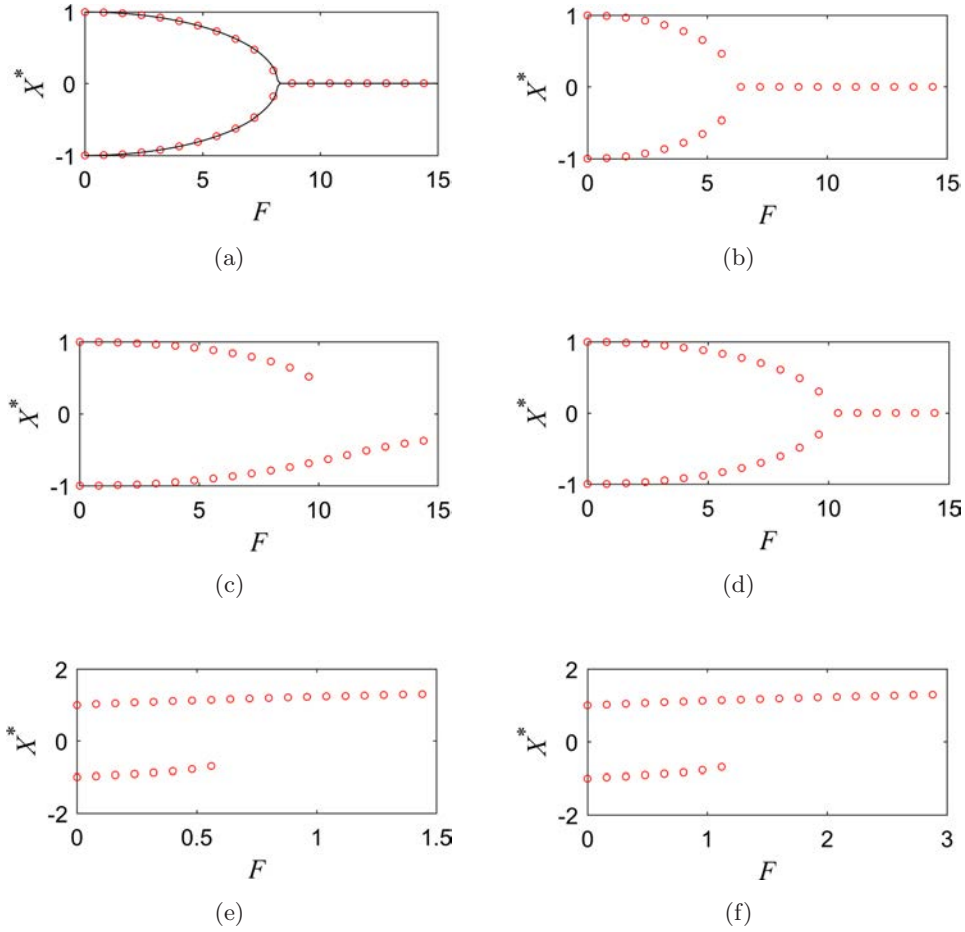


Fig. 2. The PB diagram corresponding to the six excitations given in Fig. 1 respectively.

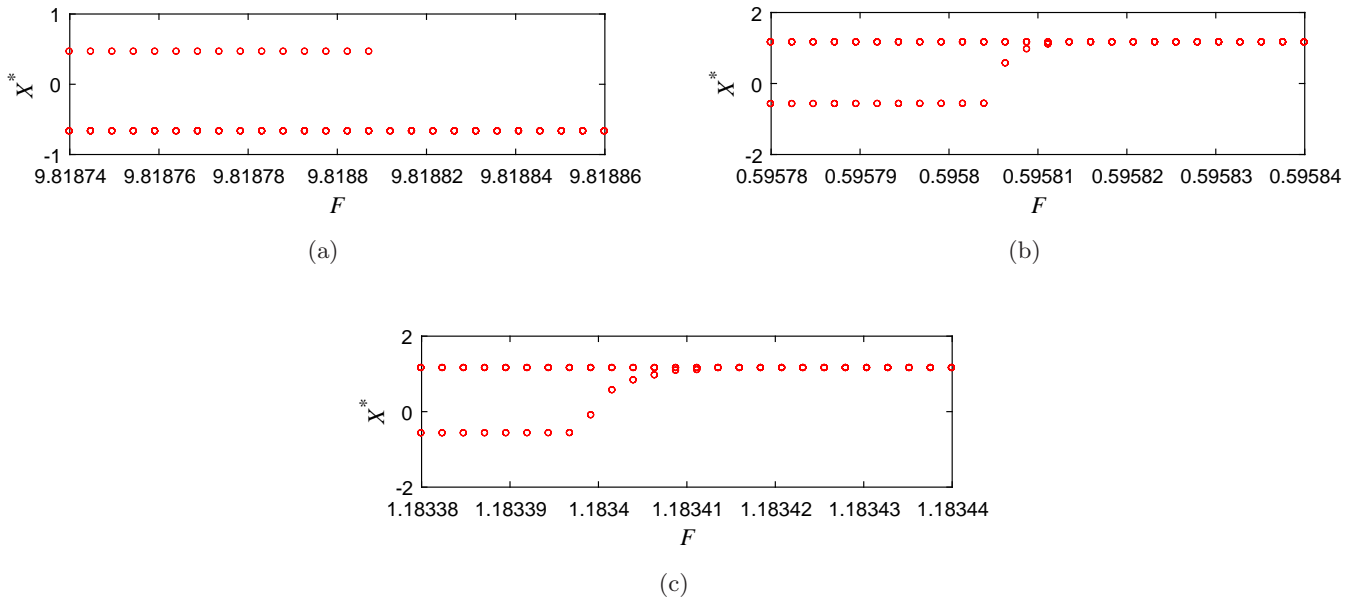


Fig. 3. Panels (a)–(c) correspond to the local enlargement of panels Figs. 2(c), 2(e), and 2(f), respectively.

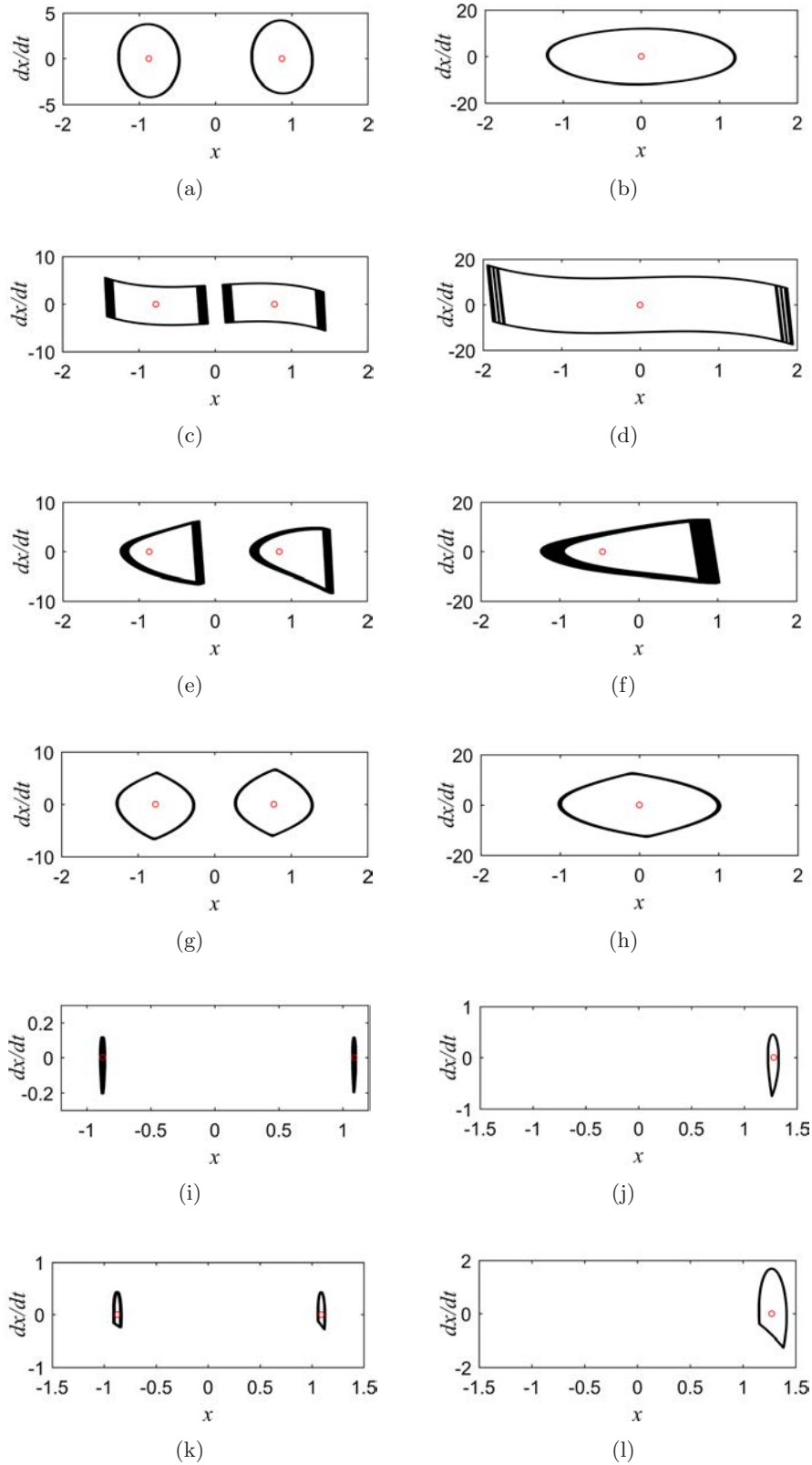


Fig. 4. The phase diagrams corresponding to different fast excitations before (left panel) and after (right panel) the bifurcation with numerically calculated equilibria (small circles). Cosine waveform excitation in (a)  $F = 4$  and (b)  $F = 12$ , square waveform excitation in (c)  $F = 4$  and (d)  $F = 12$ , asymmetric sawtooth waveform excitation in (e)  $F = 6.4$  and (f)  $F = 12.8$ , symmetric sawtooth waveform excitation in (g)  $F = 6.4$  and (h)  $F = 12.8$ , modulus of sine waveform excitation in (i)  $F = 0.32$  and (j)  $F = 1.28$ , rectified cosine waveform excitation in (k)  $F = 0.64$  and (l)  $F = 2.56$ .

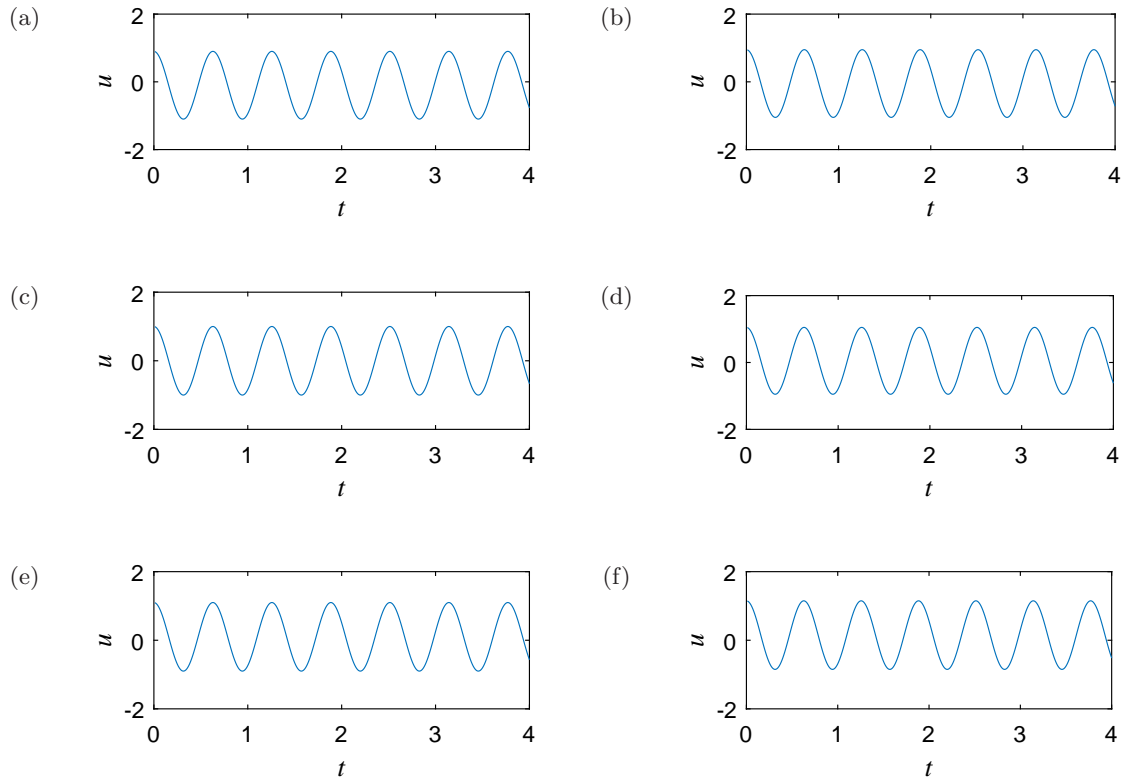


Fig. 5. The deviated cosine waveforms with different deviations. (a)  $\delta = -0.10$ , (b)  $\delta = -0.05$ , (c)  $\delta = 0$ , (d)  $\delta = 0.05$ , (e)  $\delta = 0.10$  and (f)  $\delta = 0.15$ .

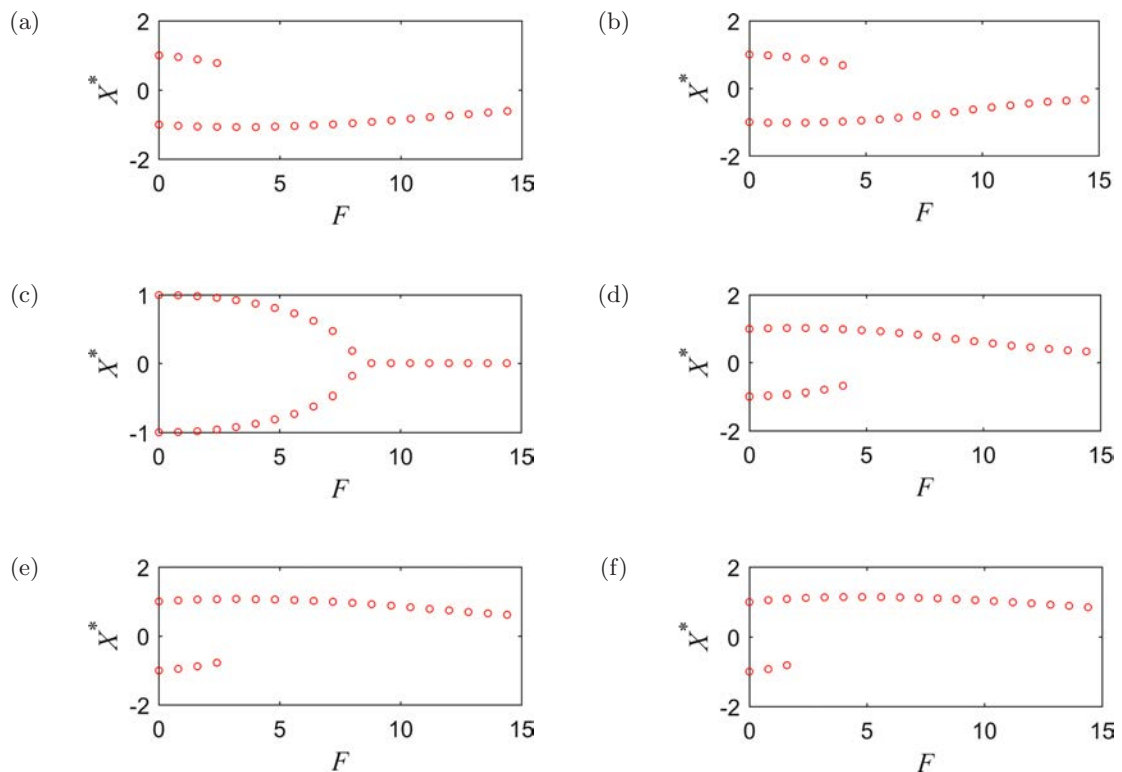


Fig. 6. The PB diagrams corresponding to six excitations given in Fig. 5 respectively.

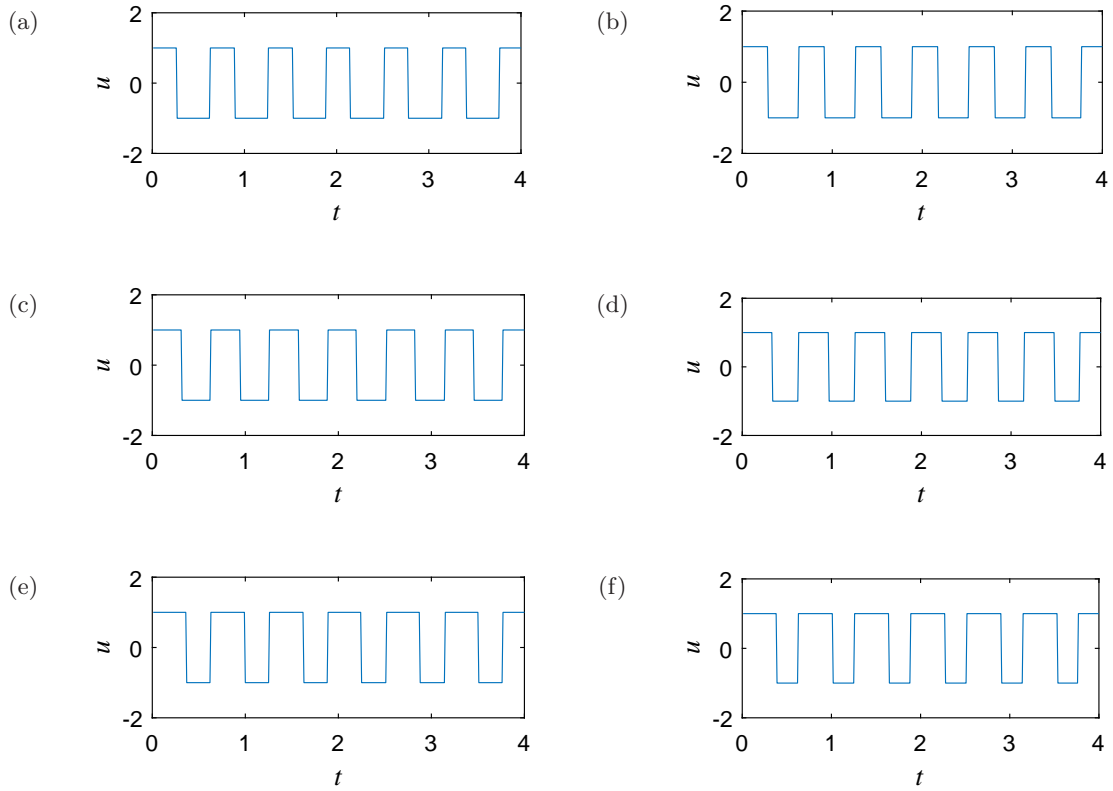


Fig. 7. Square waveform excitations with different duty cycle values. (a)  $R = 0.42$ , (b)  $R = 0.46$ , (c)  $R = 0.50$ , (d)  $R = 0.54$ , (e)  $R = 0.58$  and (f)  $R = 0.62$ .

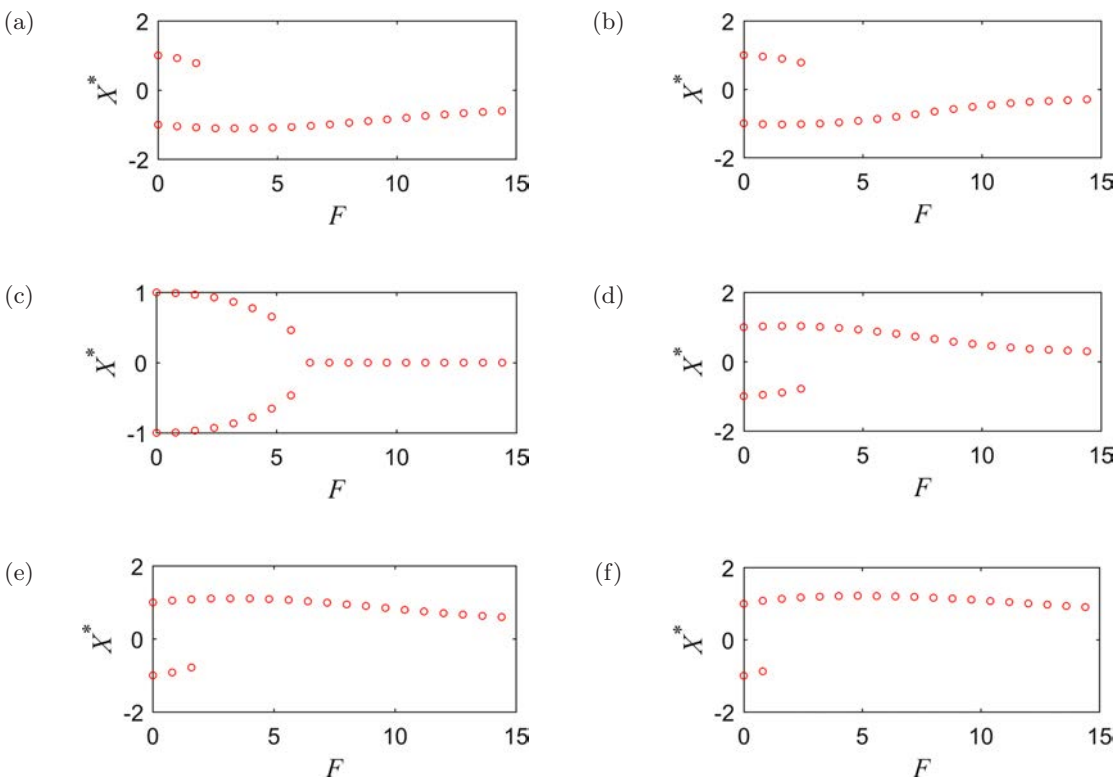


Fig. 8. The PB diagrams corresponding to the six excitations given in Fig. 7 respectively.

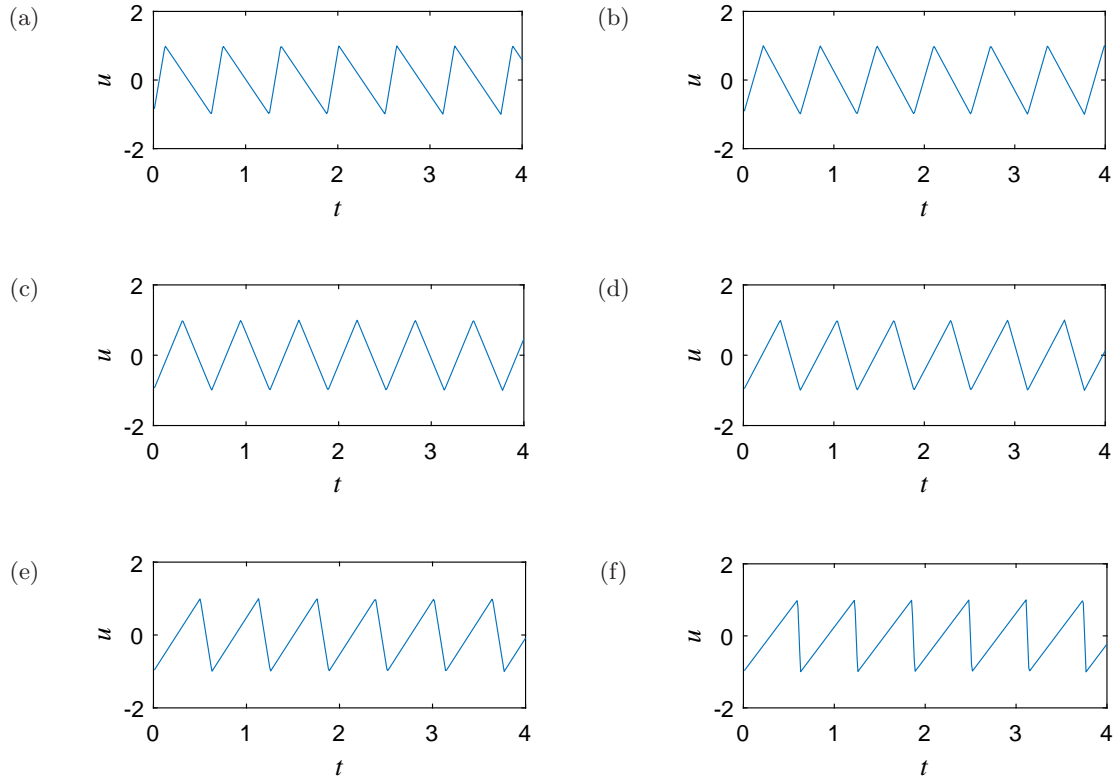


Fig. 9. Sawtooth waveforms with different rising edge slopes  $k$ . (a)  $k = \frac{2\Omega}{0.4\pi}$ , (b)  $k = \frac{2\Omega}{0.7\pi}$ , (c)  $k = \frac{2\Omega}{\pi}$ , (d)  $k = \frac{2\Omega}{1.3\pi}$ , (e)  $k = \frac{2\Omega}{1.6\pi}$  and (f)  $k = \frac{2\Omega}{1.9\pi}$ .

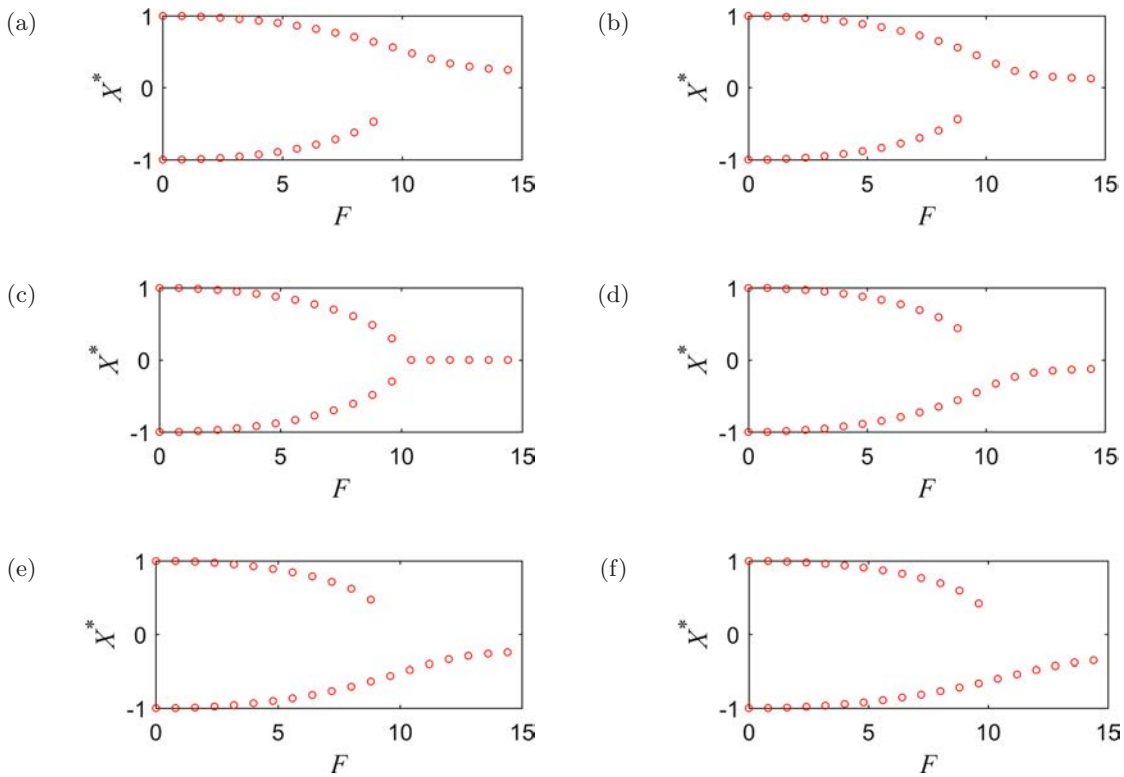


Fig. 10. The PB diagrams corresponding to the six excitations given in Fig. 9 respectively.

symmetry of the sawtooth waveform and then influence the PB configuration and the location of the PB point. With the decrease of the rising edge slope, the PB point will occur from below  $X^* = 0$  to above  $X^* = 0$ .

In this section, we find that the cosine waveform, the square waveform, the symmetric sawtooth waveform, will induce symmetric PB. However, the asymmetric sawtooth waveform, the modulus of sine waveform, the rectified cosine waveform will induce asymmetric PB. When the derivation of the cosine waveform, the duty cycle of the square waveform, the rising edge slope of the symmetric sawtooth waveform, makes the waveform itself lose the symmetric features, the symmetry of the PB diagram also breaks, and the PB point is changed.

### 3. Fast Excitation Forms on VR

In this section, we will investigate the VR induced by different fast excitations. For the special case, we will use numerical simulations verified by analytical results. For the general case, we mainly use the numerical simulations to reveal the VR phenomenon. The VR is usually measured by the response amplitude of the system at the input low-frequency, which is calculated by

$$Q = \frac{\sqrt{Q_s^2 + Q_c^2}}{f}, \quad (18)$$

where

$$\begin{cases} Q_s = \frac{2}{rT} \int_0^{rT} x(t) \sin \omega t dt, \\ Q_c = \frac{2}{rT} \int_0^{rT} x(t) \cos \omega t dt. \end{cases} \quad (19)$$

For the numerical solution, the discrete form of Eq. (19) is

$$\begin{cases} Q_s = \frac{2}{rT} \sum_{i=1}^N x(t_i) \sin \omega t_i \Delta t, \\ Q_c = \frac{2}{rT} \sum_{i=1}^N x(t_i) \cos \omega t_i \Delta t \end{cases} \quad N = \frac{rT}{\Delta t}. \quad (20)$$

If the fast periodic excitation is the harmonic function case, such as in Eq. (2), the analytical solution of the response amplitude is shown in Eq. (21)

[Yang & Zhu, 2012, Eq. (16)]

$$Q = \frac{1}{\sqrt{\left(\omega_r^2 + \omega \cos \frac{\pi}{2}\right)^2 + \left(\omega \sin \frac{\pi}{2}\right)^2}}, \quad (21)$$

where

$$\omega_r^2 = C_1 + 3bX^{*2}$$

and  $X^*$  is the stable equilibrium of the system response.

These waveforms given in Fig. 1 are used as fast excitations and the corresponding VR diagrams based on the above solutions are shown in Fig. 11. For the numerical simulations, we use all values in  $x(1) = -3 : 0.5 : 3$  as initial conditions. Apparently, the initial condition influences the configuration of the  $Q-F$  curve.

Analyzing Fig. 11 and comparing it with Fig. 2, we can see that there are some relations between the VR diagram and the bifurcation diagram. From previous works, we know that the value of  $F$  corresponding to the bifurcation point is the same as the value of  $F$  corresponding to the resonance peak. This conclusion is also satisfied even when the VR is weak such as in Figs. 11(c), 11(e) and 11(f). Fast excitations induce symmetric PB such as in Figs. 11(a), 11(b) and 11(d), which have larger  $Q$  at resonance, that is, their VR phenomenon is obvious. Conversely, fast excitations cannot induce symmetric PB such as in Figs. 11(c), 11(e) and 11(f), which have smaller  $Q$  at resonance, that is, their VR phenomenon is weak.

Besides, there are many nonoverlapping curves in Figs. 11(c), 11(e) and 11(f), which illustrate that some initial values of the system cannot induce the VR phenomenon, so it is necessary to examine the initial values of the system more accurately. Naturally, we divide the curves in Fig. 11 into three types  $x(1) < 0$ ,  $x(1) = 0$  and  $x(1) > 0$ . We find that the initial condition does influence the VR curve.

In order to further study the dependence of the VR on the initial conditions, taking the square waveforms in Fig. 7 as examples, the different VR curves are shown in Fig. 12. Comparing Figs. 12 and 8, we find that provided the bifurcation point moves up, the VR phenomenon will be induced only when the initial value of the system is less than zero. Provided the bifurcation point moves down, the VR phenomenon will be induced only when the initial value of the system is more than zero. Additionally, the nonoverlapping curves in panels (d), (e) and (f)

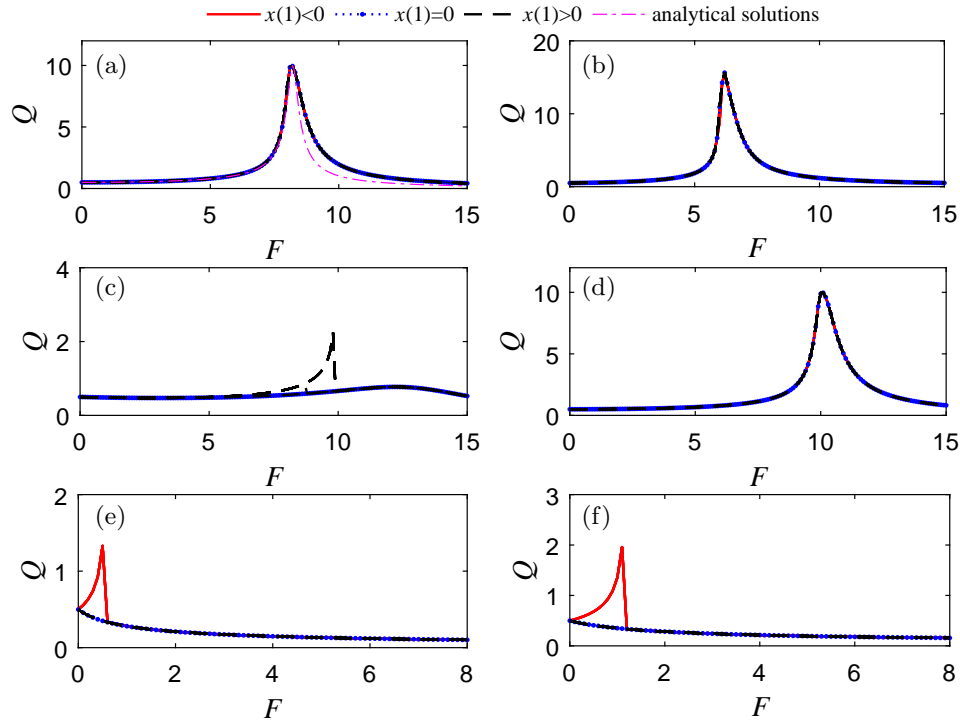


Fig. 11. The VR phenomenon. (a) Cosine waveform excitation, (b) square waveform excitation, (c) asymmetric sawtooth waveform excitation, (d) symmetric sawtooth waveform excitation, (e) modulus of sine waveform excitation and (f) rectified cosine waveform excitation. The initial conditions are all values in  $x(1) = -3 : 0.5 : 3$ .

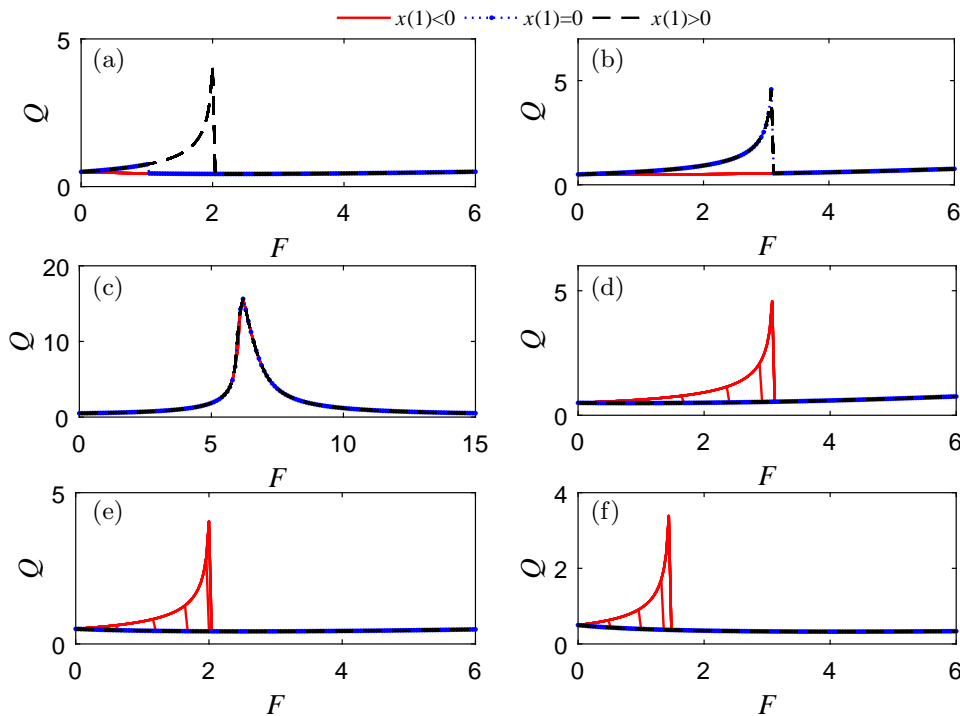


Fig. 12. The VR phenomenon induced by the waveforms in Fig. 7. (a)  $R = 0.42$ , (b)  $R = 0.46$ , (c)  $R = 0.50$ , (d)  $R = 0.54$ , (e)  $R = 0.58$  and (f)  $R = 0.62$ . The initial conditions are all values in  $x(1) = -2 : 0.2 : 2$ .

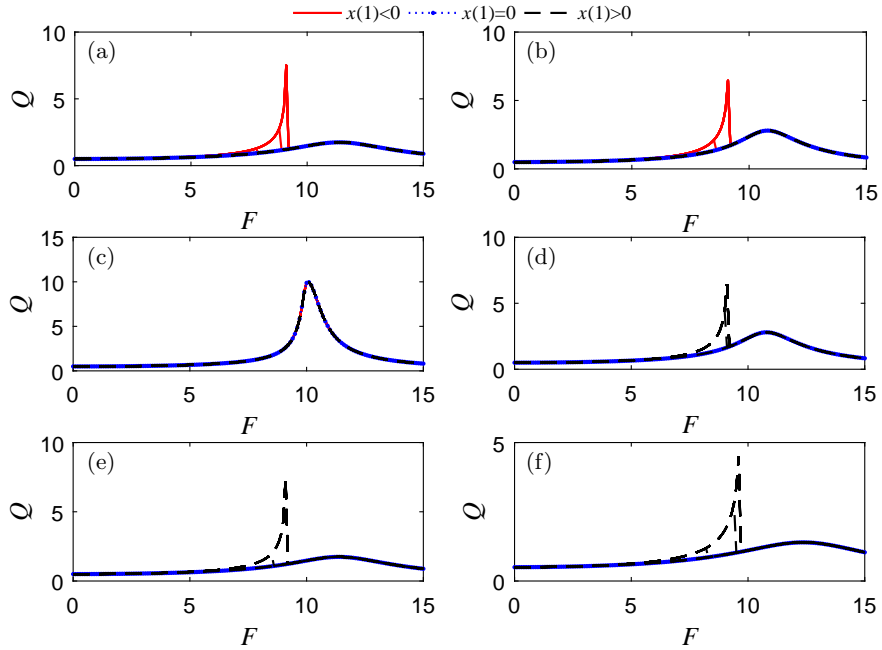


Fig. 13. The VR phenomenon induced by the waveforms in Fig. 9. (a)  $k = \frac{2\Omega}{0.4\pi}$ , (b)  $k = \frac{2\Omega}{0.7\pi}$ , (c)  $k = \frac{2\Omega}{\pi}$ , (d)  $k = \frac{2\Omega}{1.3\pi}$ , (e)  $k = \frac{2\Omega}{1.6\pi}$  and (f)  $k = \frac{2\Omega}{1.9\pi}$ . The initial conditions are all values in  $x(1) = -2 : 0.2 : 2$ .

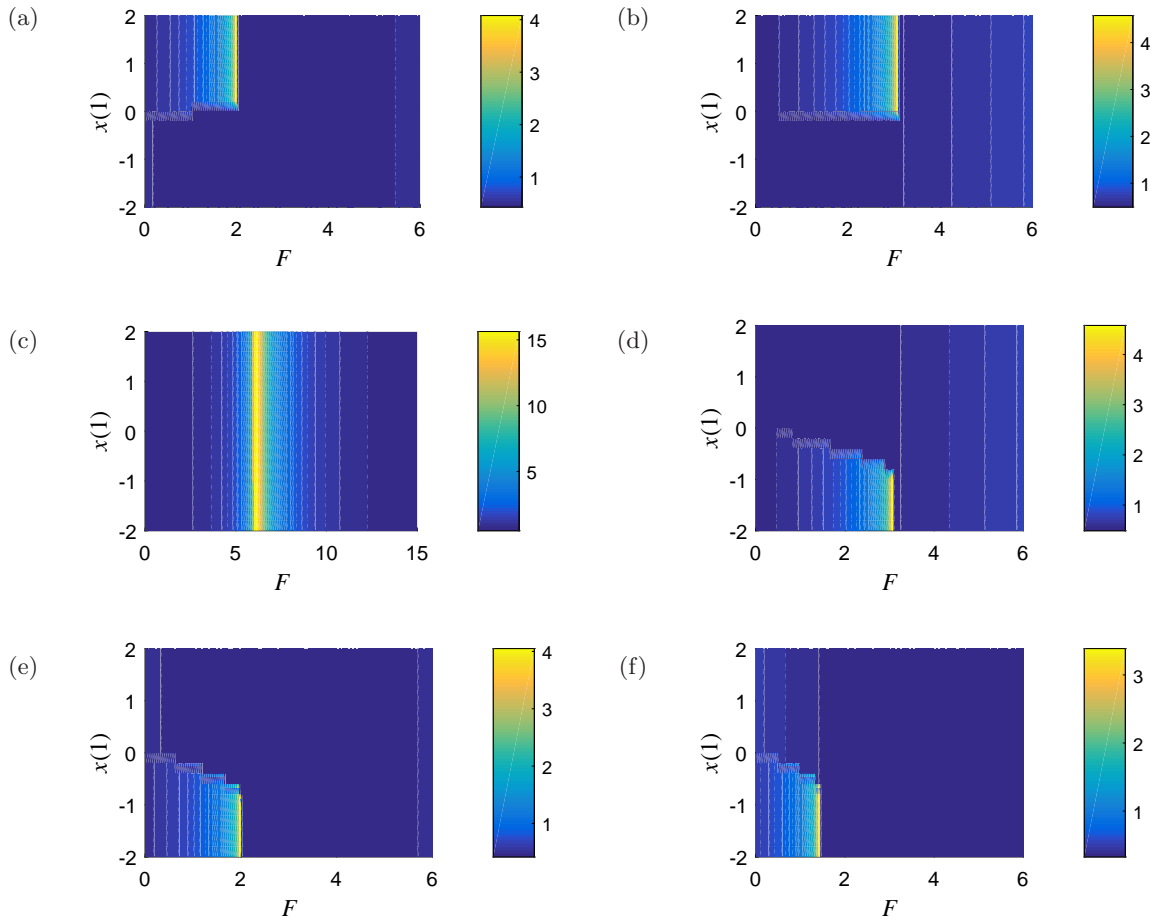


Fig. 14. The VR phenomenon induced by the waveforms in Fig. 7 and the initial condition  $x(1)$ . (a)  $R = 0.42$ , (b)  $R = 0.46$ , (c)  $R = 0.50$ , (d)  $R = 0.54$ , (e)  $R = 0.58$  and (f)  $R = 0.62$ .

in Fig. 12 indicate that when the initial value of the system gradually increases from  $-2$  to  $0$ , the VR curves gradually approach and coincide with the non-VR curves.

In Fig. 13, we give the VR curve induced by the excitations in Fig. 9, i.e. sawtooth waveforms with different rising edge slopes. We have similar results as that in Fig. 12. Specifically, the symmetry of the fast excitation and the initial condition influence the VR phenomenon greatly.

Finally, in order to make the dependence of the response amplitude on the initial value much more clear and intuitive, Fig. 14 shows the VR corresponding to the six square waveforms in Fig. 7. It can be judged that the VR induced by the square waveforms has an obvious boundary. Specifically, if the duty cycle  $R \neq 0.5$ , the VR disappears when  $x(1) < 0$  for  $R < 0.5$ , and  $x(1) > 0$  for  $R > 0.5$ . For  $R = 0.5$ , it is the standard square waveform, and the appearance of VR is independent of the initial value. Moreover, the standard square waveform can induce much stronger VR.

#### 4. Conclusions

In this paper, we have investigated the PB and VR in an overdamped bistable system when subjected under both a slow excitation and a fast excitation with different waveforms. Not any kind of fast excitation can cause the standard PB diagram of the nonlinear system. The fast excitation must satisfy certain conditions, that is, the fast excitation should have a harmonic or a symmetric waveform. Provided the fast excitation is an asymmetric waveform, the PB diagram will suddenly jump, and the bifurcation point will move up or down. Although some PB diagrams do not have an obvious jump, they also need to be magnified greatly to determine the location of the bifurcation point. Thus, the relatively great change takes place as well. If the PB diagram deforms, the initial values influence the VR curve greatly, and the VR strength will significantly reduce. By choosing an appropriate fast excitation waveform, we can better control the bifurcation and resonance of a nonlinear system.

#### Acknowledgments

The project was supported by the National Natural Science Foundation of China (Grant No. 11672325), the Key Project of National Natural Science Foundation of China (Grant No. U1510205), the Priority

Academic Program Development of Jiangsu Higher Education Institutions and the Top-notch Academic Programs Project of Jiangsu Higher Education Institutions, and by the Spanish State Research Agency (AEI) and the European Regional Development Fund (FEDER) under Project No. FIS2016-76883-P.

#### References

- Blekhman, I. I. [2000] *Vibrational Mechanics: Nonlinear Dynamic Effects, General Approach, Applications* (World Scientific, Singapore).
- Blekhman, I. I. & Landa, P. S. [2004] “Conjugate resonances and bifurcations in nonlinear systems under biharmonic excitation,” *Int. J. Non-Linear Mech.* **39**, 421–426.
- Chizhevsky, V. N. & Giacomelli, G. [2008] “Vibrational resonance and the detection of aperiodic binary signals,” *Phys. Rev. E* **77**, 051126.
- Gandhimathi, V. M., Murali, K. & Rajasekar, S. [2006] “Stochastic resonance with different periodic forces in overdamped two coupled anharmonic oscillators,” *Chaos Solit. Fract.* **30**, 1034–1047.
- Golubitsky, M. & Schaeffer, D. G. [1985] *Singularities and Groups in Bifurcation Theory*, Vol. 1 (Springer-Verlag, New York).
- Grassie, S. L., Gregory, R. W., Harrison, D. & Johnson, K. L. [1982] “The dynamic response of railway track to high frequency vertical excitation,” *J. Mech. Engin. Sci.* **24**, 77–90.
- Ji, J. C. & Leung, A. Y. T. [2002] “Bifurcation control of a parametrically excited Duffing system,” *Nonlinear Dyn.* **27**, 411–417.
- Landa, P. S. & McClintock, P. V. E. [2000] “Vibrational resonance,” *J. Phys. A: Math. Gen.* **33**, L433–L438.
- Mares, J. O., Miller, J. K., Sharp, N. D., Moore, D. S., Adams, D. E., Groven, L. J. & Son, S. F. [2013] “Thermal and mechanical response of PBX 9501 under contact excitation,” *J. Appl. Phys.* **113**, 084904.
- Nakamura, K., Fujita, K. & Ichinokura, O. [2013] “Magnetic-circuit-based iron loss estimation under square wave excitation with various duty ratios,” *IEEE Trans. Magnet.* **49**, 3997–4000.
- Popov, A. A. [2003] “Parametric resonance in cylindrical shells: A case study in the nonlinear vibration of structural shells,” *Engin. Struct.* **25**, 789–799.
- Rajasekar, S., Jeyakumari, S., Chinnathambi, V. & Sanjuán, M. A. F. [2010] “Role of depth and location of minima of a double-well potential on vibrational resonance,” *J. Phys. A: Math. Theoret.* **43**, 465101.
- Rajasekar, S., Wagemakers, A. & Sanjuán, M. A. F. [2012] “Vibrational resonance in biological nonlinear maps,” *Commun. Nonlinear Sci. Numer. Simulat.* **17**, 3435–3445.

- Rajasekar, S. & Vallejo, J. C. [2016] *Nonlinear Resonances* (Springer-Verlag, Berlin-Heidelberg-New York-Tokyo).
- Thomsen, J. J. [2008] “Effective properties of mechanical systems under high-frequency excitation at multiple frequencies,” *J. Sound Vibr.* **311**, 1249–1270.
- Ullner, E., Zaikin, A., Garcia-Ojalvo, J., Bascones, R. & Kurths, J. [2003] “Vibrational resonance and vibrational propagation in excitable systems,” *Phys. Lett. A* **312**, 348–354.
- Wang, C., Yang, K. & Qu, S. [2014] “Vibrational resonance in a discrete neuronal model with time delay,” *Int. J. Mod. Phys. B* **28**, 1450103.
- Yabuno, H., Miura, M. & Aoshima, N. [2004] “Bifurcation in an inverted pendulum with tilted high-frequency excitation: Analytical and experimental investigations on the symmetry-breaking of the bifurcation,” *J. Sound Vibr.* **273**, 493–513.
- Yabuno, H. & Tsumoto, K. [2007] “Experimental investigation of a buckled beam under high-frequency excitation,” *Arch. Appl. Mech.* **77**, 339–351.
- Yang, J. H., Sanjuán, M. A. F. & Liu, H. G. [2015] “Bifurcation and resonance in a fractional Mathieu–Duffing oscillator,” *Eur. Phys. J. B* **88**, 310.
- Yang, J. H., Huang, D., Sanjuán, M. A. F. & Liu, H. [2018] “Vibrational resonance in an overdamped system with a fractional order potential nonlinearity,” *Int. J. Bifurcation and Chaos* **28**, 1850082-1–12.
- Yang, J. H. & Zhu, H. [2012] “Vibrational resonance in Duffing systems with fractional-order damping,” *Chaos* **22**, 013112.
- Yao, C. & Zhan, M. [2010] “Signal transmission by vibrational resonance in one-way coupled bistable systems,” *Phys. Rev. E* **81**, 061129.